Journal of Solid State Chemistry **155**, 366–371 (2000)
doi:10.1006/jssc.2000.8926, available online at http://www.idealibrary.com on IDEAL®

Synthesis, Structure, Electrical Conductivity, and Band Structure of the Rare-Earth Copper Oxychalcogenide $La_5Cu_6O_4S_7$

Fu Qiang Huang,* Paul Brazis,† Carl R. Kannewurf,† and James A. Ibers*,[1]

Department of Chemistry and †Department of Electrical and Computer Engineering, Northwestern University, 2145 Sheridan Road, Evanston, Illinois 60208-3113

Received March 31, 2000; in revised form July 25, 2000; accepted August 9, 2000; published online November 29, 2000

The compound $La_5Cu_6O_4S_7$ has been synthesized by the reaction of La_2S_3 and CuO in a KI flux at 1173 K. $La_5Cu_6O_4S_7$ crystallizes in a new structure type in a cell of dimensions $a = 5.667(1)$, $b = 15.666(3)$, $c = 17.534(3)$ Å with four formula units in space group D_{2h}^{28}-*Imma* of the orthorhombic system at $T = 153$ K. The structure comprises $[Cu_2S_2]$ antifluorite-like and $[La_{10}S_2O_8]$ fluorite-like layers, and these two kinds of layers stack in turn along the [001] direction. The La atom is coordinated by a distorted square antiprism of four O and four S atoms, and the Cu atom is coordinated by a tetrahedron of four S atoms. The Cu atom in the $[Cu_2S_2]$ layer is bonded to neighboring Cu atoms; the Cu–Cu distances vary from 2.5864(7) to 2.965(1) Å. The average oxidation state of the Cu atoms is $+7/6$. $La_5Cu_6O_4S_7$ is metallic in the [100] direction, consistent with the results of extended Hückel band structure calculation. © 2000 Academic Press

INTRODUCTION

Interest in high-temperature superconductors has led to numerous studies of layered lanthanide copper oxides (1–3). However, there are very few reports of related oxychalcogenides. The compounds *Ln*CuO*Q* (*Ln* = rare earth element; *Q* = S, Se) (4–7) are known. These belong to the LaAgOS structure type (4) and contain the intergrowth of fluorite-like $[Ln_2O_2]$ and antifluorite-like $[Cu_2Q_2]$ layers. The formal oxidation state of Cu is $+1$ in these compounds, and they should all be semiconductors (8). Given the *Ln*CuO*Q* structure, if the $[Cu_2Q_2]$ layer were kept unchanged and some *Q* atoms were to replace some O atoms in the $[Ln_2O_2]$ layer, then the dimensions of the fluorite-like layer might expand with the result that the *Ln*:Cu ratio would decrease and the average oxidation state of Cu would be greater than one. This could result in more interesting physical properties.

We have successfully replaced some O atoms with S atoms in the $[Ln_2O_2]$ layer to form the compound $La_5Cu_6O_4S_7$. This compound belongs to a new structure type, but it is closely related to the *Ln*CuOS structure. The Cu atoms in $La_5Cu_6O_4S_7$ have an average oxidation state of $+7/6$ and the compound shows metallic conductivity in one direction. Here we present the synthesis, structure, electrical conductivity, and band structure calculations on $La_5Cu_6O_4S_7$.

EXPERIMENTAL

Synthesis

La_2S_3 (1.0 mmol; Strem, 97%), CuO (2.0 mmol; Alfa, 99.99%), and KI (2.4 mmol, Aldrich, 99.99 + %) were loaded into a fused silica tube under an argon atmosphere in a glove box. This tube was sealed under a 10^{-4}-Torr atmosphere and then placed in a computer-controlled furnace. The sample was heated to 1173 K at 1 K/min, kept at 1173 K for 4 days, and cooled at 0.05 K/min to 573 K; then the furnace was turned off. The reaction mixture was washed free of iodide salts with water and then dried with acetone. There were two major products: orange needles and light yellow powder. The yield of needles was about 50–60%. Analysis of the needles with an EDX-equipped Hitachi S-4500 SEM showed the presence of La, Cu, and S approximately in the molar ratio of 5:6:7; O was observed but could not be quantified. No evidence of K or I was found. The compound is $La_5Cu_6O_4S_7$, as determined by an X-ray diffraction study. It is very stable in air. Analysis of the light yellow powder gave a molar ratio La:S approximately 2:3 with no trace of O corresponding to the starting material La_2S_3.

Structure Determination

Single-crystal X-ray diffraction data were collected on a $0.032 \times 0.058 \times 0.380$-mm needle with the use of graphite-monochromatized Mo*Kα* radiation ($\lambda = 0.71073$ Å) at

---

[1] To whom correspondence should be addressed.

0022-4596/00 $35.00

153 K on a Bruker Smart-1000 CCD diffractometer (9). The crystal-to-detector distance was 5.023 cm. Crystal decay was monitored by recollecting 50 initial frames at the end of data collection. Data were collected by a scan of 0.3° in ω, respectively, in groups of 606, 606, and 606 frames at φ settings of 0°, 120°, and 240°. The exposure times were 20 s/frame. The collection of intensity data on the Bruker diffractometer was carried out with the program SMART (9). Cell refinement and data reduction were carried out with the use of the program SAINT (9) and a face-indexed absorption correction was performed numerically with the use of the program XPREP (10). The program SADABS (9) was then employed to make incident beam and decay corrections.

The structure was solved with the direct methods program SHELXS of the SHELXTL.PC suite of programs and refined by full-matrix least-squares techniques (10). The initial solution led to atom S5 in position (4*d*) $\frac{1}{4}, \frac{1}{4}, \frac{3}{4}$. The ensuing refinement, which included anisotropic displacement parameters and a secondary extinction correction, converged to an R_1 index of 0.0321 and was satisfactory in all respects save for the value of U_{11}(S5) of 0.120(3) Å^2, an extraordinarily large value for an S atom in a structure of a quaternary metal oxysulfide derived from a low-temperature data set. Accordingly, atom S5 was placed in position (8*i*) $x, \frac{1}{4}, z$ with occupancy 0.5 and $x \approx \frac{1}{4}$ and $z \approx \frac{3}{4}$. This refinement converged to a value of R_1 of 0.0310 and to U_{11}(S5) = 0.021(3) Å^2. The principal mean-square atomic displacements for atom S5 are not exceptional compared with those of other atoms in the structure. The S5 chains along *a* must be ordered; otherwise impossibly short S5–S5 distances of 0.539(6) Å result. The disorder of the S5 positions arises from the lack of interchain communication, since no evidence of a supercell was found. Additional experimental details are shown in Table 1. Table 2 gives positional parameters and equivalent isotropic displacement parameters and Table 3 presents selected bond distances.

Electrical Conductivity

The composition of two orange single crystals of $La_5Cu_6O_4S_7$ was confirmed with EDX measurements. The electrical conductivity of the single crystal samples was measured with the use of a computer-controlled, four-probe technique (11). Electrical contacts consisted of fine gold wire (25 and 60 μm in diameter) attached to the crystals with gold paste. Samples were placed under vacuum for at least 24 h to allow the gold paste to cure completely, which improved contact performance. Excitation currents were kept as low as possible, typically below 1 mA, in order to minimize any nonohmic voltage response and thermoelectric effects at the contact–sample interface. Measurements of the sample cross-sectional area and voltage probe separation were made with a calibrated binocular microscope.

TABLE 1
Crystal Data and Structure Refinement for $La_5Cu_6O_4S_7$

Formula weight	1364.21
Space group	*Imma*
a (Å)	5.667(1)
b (Å)	15.666(3)
c (Å)	17.534(3)
Volume (Å^3)	1556.8(5)
Z	4
T (K)	153 (2)
λ (Mo*K*α)	0.71073
ρ_c (g/cm^3)	5.821
Crystal dimensions (mm)	0.032 × 0.058 × 0.380
μ (cm^{-1})	223.37
Transmission factors	0.102–0.537
Total reflections/unique reflections	6527/1071
Extinction coefficient	0.00023(4)
Maximum/minimum difference density (e/Å^3)	4.4(4)/–2.3(4)
$R(F)^a$ ($F_0^2 > 2\sigma(F_0^2)$)	0.0310
R_w $(F_0^2)^b$ (all data)	0.0826

[a] $R(F) = \sum||F_0|-|F_c||/\sum|F_0|$.

[b] R_w $(F_0^2) = [\sum w(F_0^2 - F_c^2)^2/\sum wF_0^4]^{1/2}$, $w^{-1} = \sigma^2(F_0^2) + (0.04 \times F_0^2)^2$ for $F_0^2 > 0$; $w^{-1} = \sigma^2(F_0^2)$ for $F_0^2 \leq 0$.

Extended Hückel Calculations

Calculations were performed on a tetrahedral CuS_4^{7-} fragment, one $[Cu_2S_2^{2-}]$ layer in LaCuOS, and one $[Cu_2S_2^{5/3-}]$ layer in $La_5Cu_6O_4S_7$ with the use of the YAeHMOP package (12–14). These calculations were each carried out only on one layer in the corresponding unit cell. The parameters used for Cu and S orbitals are listed in Table 4.

TABLE 2
Atomic Coordinates and Equivalent Isotropic Displacement Parameters for $La_5Cu_6O_4S_7$

Atom	*x*	*y*	*z*	U_{eq} (Å^2)^a
La1	0.0000	0.06913(2)	0.17849(2)	0.0060(2)
La2	0.0000	0.10397(2)	0.66725(2)	0.0093(2)
La3	0.0000	0.2500	0.32132(3)	0.0057(2)
Cu1	0.2384(1)	0.16454(3)	0.01184(4)	0.0180(2)
Cu2	0.2462(1)	0.0000	0.0000	0.0179(2)
S1	0.0000	0.07297(9)	0.4099(1)	0.0083(3)
S2	0.0000	0.5917(1)	0.08004(9)	0.0094(3)
S3	0.0000	0.2500	0.0959(1)	0.0080(4)
S4	0.0000	0.2500	0.5591(1)	0.0093(4)
S5^b	0.2033(6)	0.2500	0.7528(5)	0.014(1)
O1	0.2500	0.1573(2)	0.2500	0.008(1)
O2	0.2500	0.5299(3)	0.2500	0.0088(8)

[a] U_{eq} is defined as one third of the trace of the orthogonalized U_{ij} tensor.

[b] The occupancy of atom S5 is 0.50.

TABLE 3
Selected Bond Lengths (Å) for $La_5Cu_6O_4S_7$

La1–O1 × 2	2.343(2)	La3–S3 × 2	3.183(1)
La1–O2 × 2	2.446(3)	Cu1–S1	2.477(1)
La1–S2	3.054(2)	Cu1–S2	2.393(1)
La1–S3	3.182(1)	Cu1–S3	2.407(1)
La1–S1 × 2	3.231(1)	Cu1–S4	2.353(1)
La2–O2 × 2	2.337(2)	Cu2–S1 × 2	2.422(1)
La2–S1	3.085(2)	Cu2–S2 × 3	2.445(1)
La2–S2 × 2	3.2257(9)	Cu1–Cu1	2.678(1)
La2–S4	2.971(2)	Cu1–Cu1	2.702(1)
La2–S5	2.969(5)	Cu1–Cu1	2.965(1)
La2–S5	3.166(4)	Cu2–Cu2	2.791(2)
La3–O1 × 4	2.383(2)	Cu2–Cu2	2.876(2)
La3–S1 × 2	3.179(1)	Cu1–Cu2	2.5865(7)

TABLE 4
Atomic Parameters Used for the Extended Hückel Calculations

Element	Orbital	H_{ii} (eV)	ζ_1	ζ_2	C_1	C_2
Cu	4*s*	− 11.40	2.20			
	4*p*	− 6.06	2.20			
	4*d*	− 14.00	5.95	2.30	0.5933	0.5744
S	5*s*	− 20.0	2.122			
	5*p*	− 14.0	1.827			

RESULTS AND DISCUSSION

The unit cell of $La_5Cu_6O_4S_7$ is displayed down the [100] direction in Fig. 1. This structure is related to the *Ln*Cu*OQ* structure (*Ln* = rare-earth element; Q = S, Se) (Fig. 2), which belongs to the LaAgOS structure type. *Ln*Cu*OQ* is built from $[Ln_2O_2]$ fluorite-like and $[Cu_2Q_2]$ antifluorite-like layers interstacked along [001] of a tetragonal cell. $La_5Cu_6O_4S_7$ is also built from fluorite-like $[La_{10}O_8S_2]$ and antifluorite-like $[Cu_2S_2]$ layers interstacked along [001] of an orthorhombic cell. The $[La_{10}O_8S_2]$ layer can be obtained conceptually from the $[La_2O_2]$ layer by the substitution of every fifth O atom by a S5 atom along the [010] direction, as shown in Fig. 1. When these larger S5 atoms replace the smaller O atoms, the layer is distorted, the symmetry of the structure is reduced from *P*4/*nmm* to *Imma*, and the La:Cu ratio decreases from 1:1 to 5:6.

In *Ln*Cu*OQ*, the coordination polyhedra of the *Ln* and S atoms are distorted square antiprisms with four O atoms in one base and four S atoms in another base for *Ln*, and with four Cu atoms in one base and four La atoms in another base for Q. The Cu and O atoms are coordinated tetrahedrally to four Q atoms and to four *Ln* atoms, respectively, with the tetrahedra sharing edges to form a layer. In $La_5Cu_6O_4S_7$, there are three crystallographically independent La, two Cu, five S, and two O atoms. The coordination

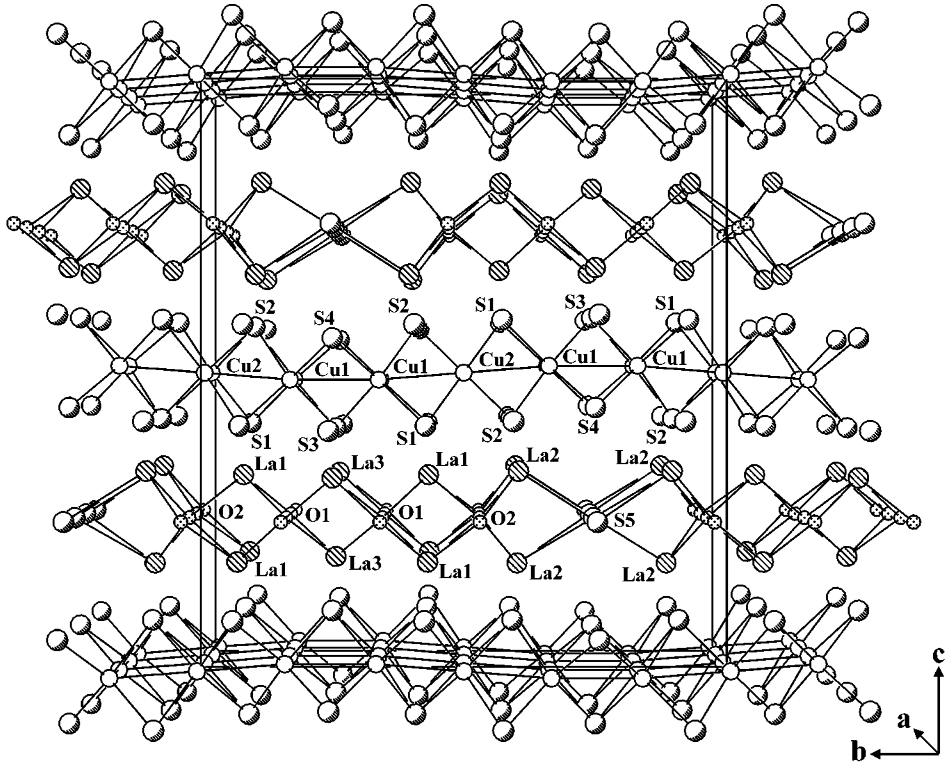

FIG. 1. Unit cell of $La_5Cu_6O_4S_7$ viewed down [100]. For clarity, no La–S bonds except La–S5 are shown.

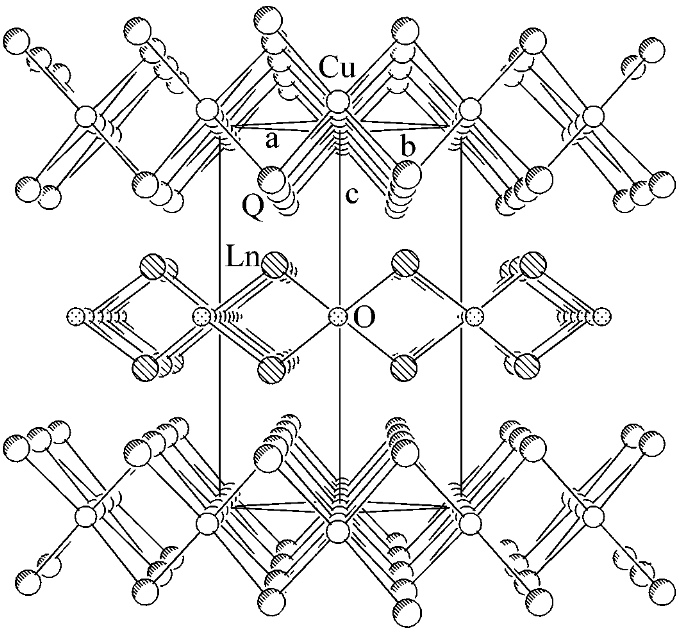

FIG. 2. Unit cell of *Ln*CuO*Q* viewed down [110]. For clarity, no *Ln*–*Q* interactions are shown.

environments for La, Cu, S, and O atoms are the same as those in *Ln*CuO*Q* except atom La2 is coordinated to six S atoms and two O atoms. The distances of La–O (2.337(2) to 2.446(3) Å), La–S (2.969(5) to 3.231(1) Å), and Cu–S (2.353(1) to 2.477(1) Å) are comparable to those in LaCuOS (La–O, 2.367(3); La–S, 3.253(4); and Cu–S, 2.437(4) Å, respectively) (7).

Figure 3 is a projection down [001] of the $[Cu_2S_2]$ layer in $La_5Cu_6O_4S_7$. As is evident from Fig. 1, this layer is distorted; the Cu1 atoms alternately shift up and down 0.208 Å from the plane of the Cu2 atoms, presumably because the S5 atoms occupy more space than the O atoms they replaced. The Cu–Cu distance of 2.827(1) Å in LaCuOS (7) now takes on six different distances, 2.678(1), 2.702(1), and 2.965(1) Å for Cu1–Cu1, 2.5865(7) Å for Cu1–Cu2, and 2.791(2) and 2.876(2) Å for Cu2–Cu2 in $La_5Cu_6O_4S_7$, as shown in Fig. 3. Similar $[Cu_2Q_2]$ layers are also found in a number of ternary $ACu_{2n}Q_{n+1}$ (A = Tl, K, Rb, Cs; Q = S, Se, Te) and $BaCu_2S_2$ compounds, where unique, short Cu–Cu distances between 2.67 and 2.89 Å are found (8, 15–19). The formal oxidation state of Cu is $+1$ in *Ln*CuO*Q*, $+1$ in $BaCu_2S_2$, and $+(2n+1)/2n$ in $ACu_{2n}Q_{n+1}$, whereas it is $+7/6$ in $La_5Cu_6O_4S_7$.

The electrical conductivity as a function of temperature of $La_5Cu_6O_4S_7$ in the [100] direction is shown in Fig. 4. The material is a metallic conductor in this direction. The increased slope below 175 K probably results from the temperature-dependent distortion of the Cu net. The conductivity of $La_5Cu_6O_4S_7$ is 2.6×10^4 S/cm at room temperature, which may be compared with the range 4.0×10^1 to 4.3×10^4 S/cm for the compounds $ACu_{2n}Q_{2n+1}$ (A = Tl, K, Rb, Cs; Q = S, Se, Te) (15–19).

Extended Hückel calculations have been performed on the hypothetical tetrahedral $3d^{10}$ CuS_4^{7-} molecular fragment, the two-dimensional $[Cu_2S_2^{2-}]$ layer in LaCuOS, and

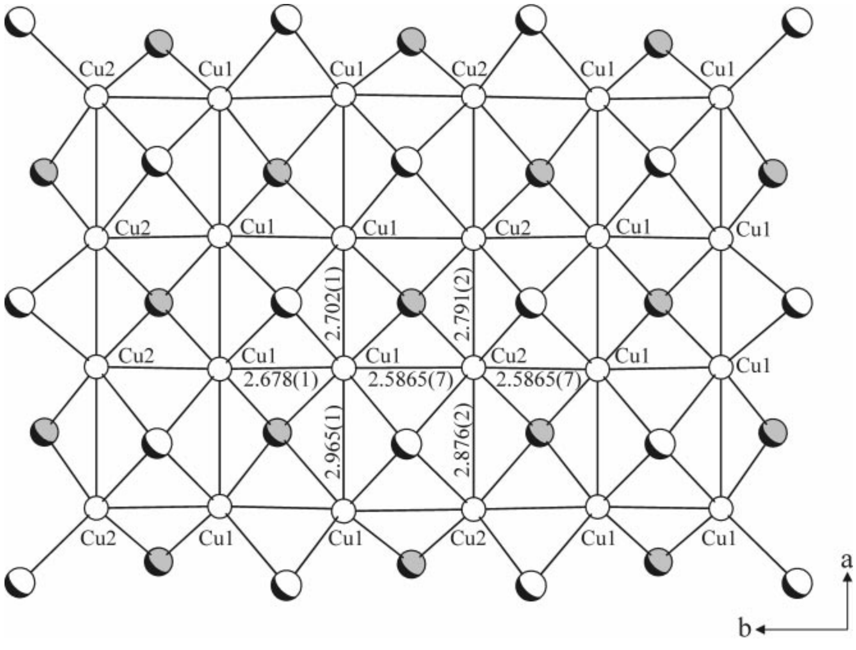

FIG. 3. Projection down [001] of the $[Cu_2S_2]$ layer in $La_5Cu_6O_4S_7$. The bottom-shaded circles represent the S atoms above the Cu net, and the bottom-shaded grey circles represent the S atoms below the Cu net.

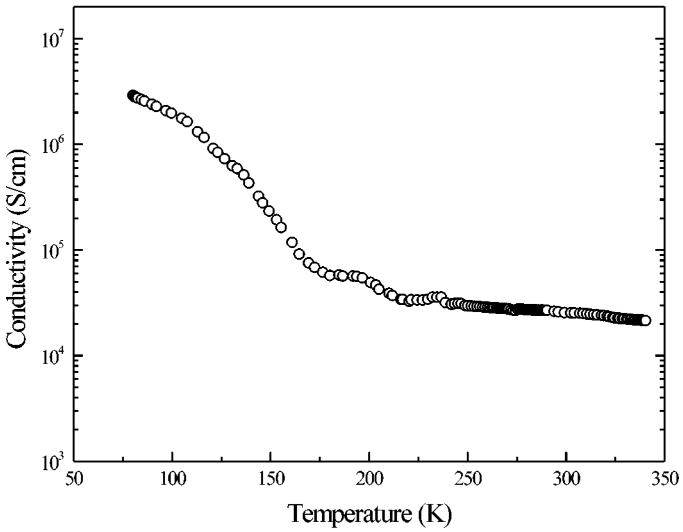

FIG. 4. Single-crystal electrical conductivity σ vs T for $La_5Cu_6O_4S_7$ along the [100] direction.

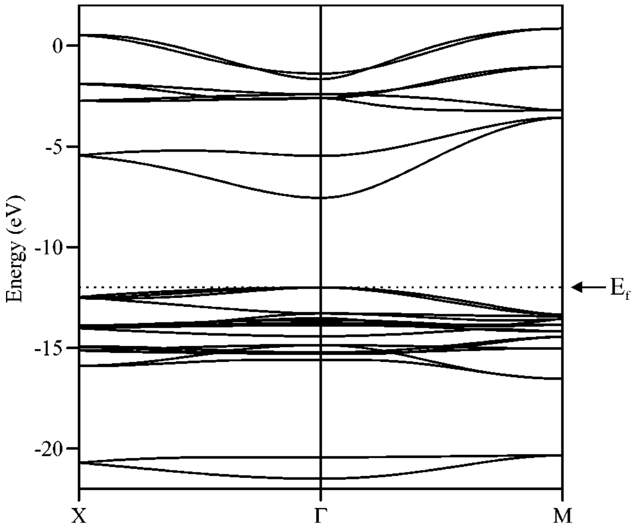

FIG. 5. The band structure of the $[Cu_2S_2^{2-}]$ layer in LaCuOS, where Γ, X, and M are (0,0,0), ($\frac{1}{2}$,0,0), and ($\frac{1}{2}$,$\frac{1}{2}$,0).

the $[Cu_2S_2^{5/3-}]$ layer in $La_5Cu_6O_4S_7$, where the CuS_4 tetrahedron is the building block of a $[Cu_2S_2]$ layer. In the tetrahedral coordination environment, five Cu 3*d* atomic orbitals (AO) are split into a typical "two below three" (Cu *e* below Cu t_2) (8, 19). The calculations on CuS_4^{7-} including and excluding Cu 3*d* orbitals result in similar Cu–S overlap populations, which are 0.32 and 0.33, respectively. Thus, Cu 3*d* *A*Os are almost nonbonding with the *A*Os of S and the strong covalent bonding between Cu and S results mainly from the interaction of the vacant Cu 4*s* and 4*p* *A*Os with occupied S 3*s* and 3*p* *M*Os (8). The calculations also indicate that the Cu 3*d* *A*Os (t_2) in CuS_4^{7-} are all occupied around the Fermi surface.

The band structure of the $[Cu_2S_2^{2-}]$ layer is shown in Fig. 5. The HOMO and LUMO energy levels in $[Cu_2S_2^{2-}]$ are -11.99 and -7.54 eV, respectively, whereas in tetrahedral CuS_4^{7-} they are -12.78 eV and -3.61 eV, respectively. The gap between the HOMO and the LUMO, 4.44 eV in $[Cu_2S_2^{2-}]$, is much narrower than that of 9.17 eV in tetrahedral CuS_4^{7-}. In comparison, the narrower gap of 4.2 eV found in the $[Cu_2S_2^{2-}]$ layer of $BaCu_2S_2$ (8) is reasonable since in $BaCu_2S_2$ the layer is slightly more compressed (the length of *a* being 3.908(1) Å in $BaCu_2S_2$ and 3.999(1) Å in LaCuOS). The insulating behavior of LaCuOS is indicated, as shown in Fig. 5.

Although the short Cu–Cu distances (e.g., 2.827(1) Å in LaCuOS and 2.763(1) Å in $BaCu_2S_2$) could indicate Cu–Cu bonding, both Cu–Cu bonding and antibonding 3*d* states are occupied in the valence bands. Only a very small positive Cu–Cu overlap population (0.012) was found; this results from second-order mixing of the Cu 4*s* and 4*p* bonding states in the occupied levels. Consider the $[Cu_2S_2^{2x-}]$ layer $(0 \leq x \leq 1)$. If $x = 1$ then all Cu $3d^{10}$ *A*Os are occupied; if $x = 0$ then the oxidation state of Cu is $+2$ and its electronic configuration is $3d^9$; if $0 < x < 1$ then Cu has a $3d^{9+x}$ configuration. As *x* decreases, the Fermi level drops (Fig. 5), some Cu–Cu antibonding 3*d* states become unoccupied, the Cu–Cu interactions become bonding, and the layer becomes metallic. The $[Cu_2S_2^{5/3-}]$ layer in $La_5Cu_6O_4S_7$ is such an example. Its band structure is similar to that of $[Cu_2S_2^{2-}]$, except for some bands that split as a result of the lower symmetry. The HOMO energy falls slightly to -12.11 eV compared with that of -11.99 eV in LaCuOS. As shown in Fig. 6, $La_5Cu_6O_4S_7$ is metallic along the [100] direction, as

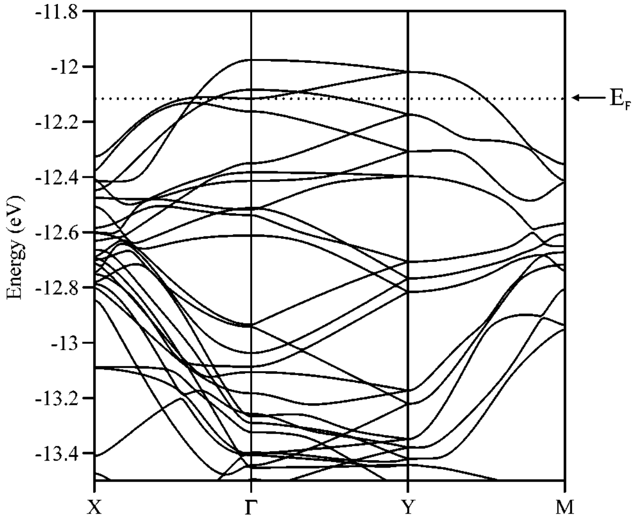

FIG. 6. The partial band structure of the $[Cu_2S_2^{5/3-}]$ layer in $La_5Cu_6O_4S_7$, where Γ, X, Y, and M are (0,0,0), ($\frac{1}{2}$,0,0), (0,$\frac{1}{2}$,0), and ($\frac{1}{2}$,$\frac{1}{2}$,0).

is found experimentally, and along [010], a direction in which the conductivity could not be measured owing to the habit of the crystals.

ACKNOWLEDGMENTS

This research was supported by NSF Grant DMR97-09351. Use was made of the Central Facilities supported by the MRSEC program of the National Science Foundation (DMR96-32472) at the Materials Research Center of Northwestern University. P.B. was supported by NSF Grant DMR96-32472.

REFERENCES

1. S. E. Barnes, J. Ashkenazi, J. L. Cohn, and F. Zuo (Eds.), "High Temperature Superconductivity," American Institute of Physics, Woodbury, New York, 1999.
2. H. A. Blackstead and J. D. Dow, *Phys. Rev. B* **55,** 6605–6611 (1997).
3. P. H. Hor, R. L. Meng, C. W. Chu, M. K. Wu, E. Zirngiebl, J. D. Thompson, and C. Y. Huang, *Nature* (*London*) **326,** 669–670 (1987).
4. M. Palazzi and S. Jaulmes, *Acta Crystallogr. B* **37,** 1337–1339 (1981).
5. P. S. Berdonosov, A. M. Kusainova, L. N. Kholodkovskaya, V. A. Dolgikh, L. G. Akselrud, and B. A. Popovkin, *J. Solid State Chem.* **118,** 74–77 (1995).
6. W. J. Zhu, Y. Z. Huang, C. Dong, and Z. X. Zhao, *Mater. Res. Bull.* **29,** 143–147 (1994).
7. M. Palazzi, *C. R. Acad. Sci. Sér. 2* **292,** 789–791 (1981).
8. A. Ouammou, M. Mouallem-Bahout, O. Peña, J.-F. Halet, J.-Y. Saillard, and C. Carel, *J. Solid State Chem.* **117,** 73–79 (1995).
9. SMART, Version 5.054, Data Collection and SAINT-Plus, Version 6.02A, Data Processing Software for the SMART System, Bruker Analytical X-Ray Instruments, Inc., Madison, WI, 2000.
10. G. M. Sheldrick, SHELXTL DOS/Windows/NT, Version 5.10, Bruker Analytical X-Ray Instruments, Inc., Madison, WI, 1997.
11. J. W. Lyding, H. O. Marcy, T. J. Marks, and C. R. Kannewurf, *IEEE Trans. Instrum. Meas.* **37,** 76–80 (1988).
12. G. Landrum, Yet Another Extended Hückel Molecular Orbital Package (YAeHMOP), Version 2.0, 1997.
13. R. Hoffmann, *J. Chem. Phys.* **39,** 1397–1412 (1963).
14. M.-H. Whangbo and R. Hoffmann, *J. Am. Chem. Soc.* **100,** 6093–6098 (1978).
15. L. Karlsson, M. P. Keane, and R. Berger, *J. Less-Common Met.* **166,** 353–365 (1990).
16. J. C. W. Folmer and F. Jellinek, *J. Less-Common Met.* **76,** 153–162 (1980).
17. R. Berger, *J. Less-Common Met.* **147,** 141–148 (1989).
18. K. Klepp, H. Boller, and H. Völlenkle, *Monatsh. Chem.* **111,** 727–733 (1980).
19. G. V. Vajenine and R. Hoffmann, *Inorg. Chem.* **35,** 451–457 (1996).